APPLICATION OF MAGNETIC MARKERS FOR PRECISE MEASUREMENT OF MAGNETIC FIELDS IN RAMPED ACCELERATORS

M. BENEDIKT*, F. CASPERS and M. LINDROOS

*Organisation Europeenne Pour La Recherche Nucleaire, CERN,
PS Division, 1211 Geneva 23, Switzerland*

For precise measurements of the magnetic field in ramped machines, different magnetic markers are in use. The best known are peaking strips, Nuclear Magnetic Resonance (NMR) probes and Electron Spin Resonance (ESR) probes. Their operational principles and limitations are explained and some examples of recent and new applications are given. A fuller theoretical description is given of the lesser-known Ferrimagnetic Resonance (FMR) probe and its practical application. The essential purpose of these magnetic markers is the *in situ* calibration of either on-line magnetic field measurements (e.g. via a magnetic pick-up coil) or field predictions (e.g. using a magnetic model).

1 INTRODUCTION

The increasing need for improved magnetic field quality in ramped machines has led to advances in both the control of power supplies and the precision of magnetic field measurements. This paper concentrates on the improvement of magnetic measurements by the use of magnetic markers. There are two basically different ways to determine the magnetic field in ramped machines. One approach is the use of a software

---

* Corresponding author. E-mail: Michael.Benedikt@cern.ch.

magnetic model to calculate and predict the magnetic field via the regulation of the power converter. The other method is based on a signal originating from a pick-up coil in a reference magnet. Both methods have their own advantages and disadvantages, but practical experience over recent years has shown that the use of magnetic markers can lead to significant improvements in either case. The magnetic model approach has, depending on its complexity, a number of poorly determined parameters and the use of markers provides additional information to calibrate these constants. When using a pick-up coil in a reference magnet, classical problems are the long term stability of the gain and the base-line offset of the integrator. Figure 1 shows schematically the application of magnetic markers, combined with the coil measurement and/or magnetic model approach for the up-ramp of a machine.

The scheme shown in Figure 1 has already been successfully used since 1988 in the CERN SPS to handle the kind of difficulty mentioned above.[1] In the following, three types of magnetic markers namely the peaking strip, the NMR and the FMR will be discussed in more detail.

Hall probes can reach a long term stability and accuracy of 10^{-4} for DC and low frequency fields ($< 50\,\text{Hz}$) but the precision is limited to 0.1% at 10 kHz and 1% at 80 kHz.[2] For that reason, as well as for the critical alignment, Hall sensors will not be considered here as reference markers.
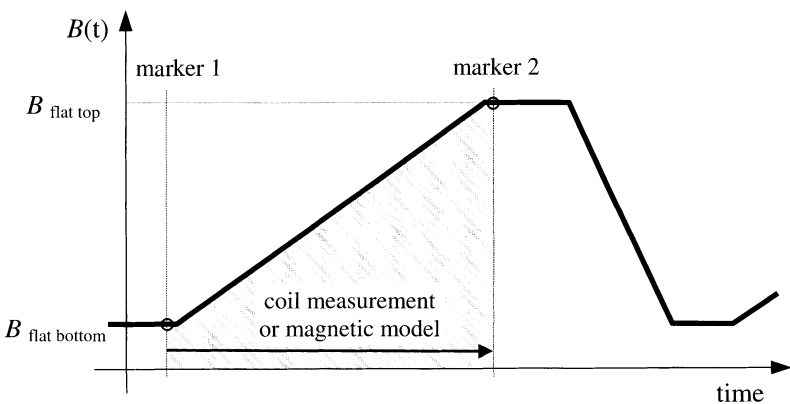

FIGURE 1   Use of magnetic markers in a ramped machine cycle.

2 BASIC THEORY OF MAGNETIC MARKERS

2.1 Peaking Strip

The classic magnetic marker used in the accelerator environment is the peaking strip also known as "fluxgate magneto-meter". This is essentially a magnetic, null detector made from a mechanically pre-stressed wire of a specific ferromagnetic material.[3-5] The pre-stress is required to create a very narrow (in ΔH), yet high (in ΔB) hysteresis loop, centred at $H = 0$. The pre-stressed wire, sometimes referred to as a "magnetic needle" or "strip", is surrounded by two coaxial, solenoidal coils which allow the adjustment of the offset field (typically -200 to 200 G, which is generally limited by thermal dissipation in the DC-operated compensation coil) with respect to the external field to be measured. These two coils with opposite but unequal fields create a fast decay of the external fringing field for the complete set-up. Due to the technical limitations of the biasing coil and the strip material this kind of detector is not suitable for operation above a few hundred Gauss. It should also be noted that the peaking strip is sensitive only to a magnetic field component in the direction of the magnetic needle.

2.2 Nuclear Magnetic Resonance

Nuclear Magnetic Resonance (NMR) based instrumentation with small sized probes (less than ~ 5 mm diameter of the active material) has a lower field limit of typical 400 G and thus is just complementary to the peaking strip in terms of B-field range. The physical principle of NMR probes is the excitation of the precession movement of the proton spin in a hydrogen nucleus.[6] The precession frequency is related to the external magnetic field by the gyro-magnetic ratio which is 4.2576396 MHz/kG for protons in water[†] at 25°C.[7] In general NMR probes require a homogeneous bias magnetic field across the active volume in order to obtain a response from all spins at the same frequency. When this condition is not met, the response is "smeared out" over a considerably wider frequency range, causing a strong attenuation of the observed

---

[†] For other commonly used plastic or rubber-like sample materials corrections in the order of a few ppm apply.
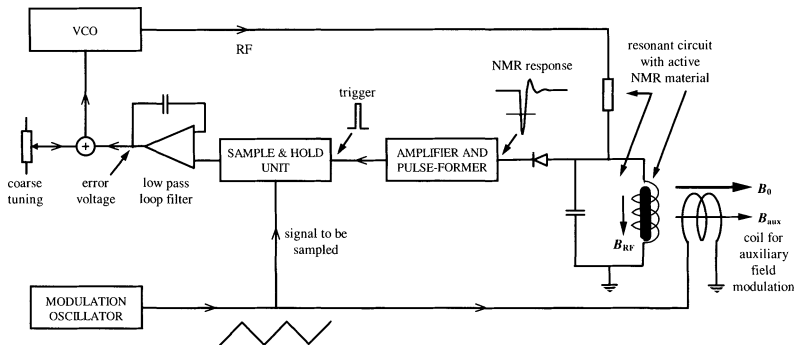
FIGURE 2   Simplified block diagram of an NMR Teslameter.

signal. This excludes the application of NMR probes in inhomogeneous fields as occur for example in quadrupole magnets.

A simplified block diagram of an NMR Teslameter, similar to the one described in Ref. 8, is depicted in Figure 2.

A Voltage Controlled Oscillator (VCO) delivers an RF signal to a low-Q resonant circuit which contains the active material in its coil. This resonant circuit is tuned to track the frequency of the VCO. As mentioned above, the precession frequency of the protons in the active material depends only on the total magnetic field at the probe location. In general, this total field is given by the superposition of the external field (to be measured) plus a contribution from an auxiliary modulation coil nearby. This auxiliary modulation coil receives a triangular-shaped excitation from a modulation oscillator and subsequently generates a triangular-shaped time varying field $B(t)$ at the location of the active material. The frequency of this modulation is typically between 10 and 200 Hz and can be manually adjusted. The amplitude of this modula-tion has typically a peak-to-peak value of 10^{-3} of the static B-field to be measured. However, it can also be set manually to larger values or be turned off according to the specific requirements. In Figure 3, the superimposed traces of both the triangular-shaped (auxiliary) mod-ulation and the NMR response are shown.

The final steady-state situation obtained after the fine tuning of the VCO is on the right side in Figure 3. Here the NMR response coincides with the zero-crossing of the triangular field modulation. At this stage, the frequency of the VCO is stable and is measured with a digital counter to give the value of the magnetic field being measured. It should
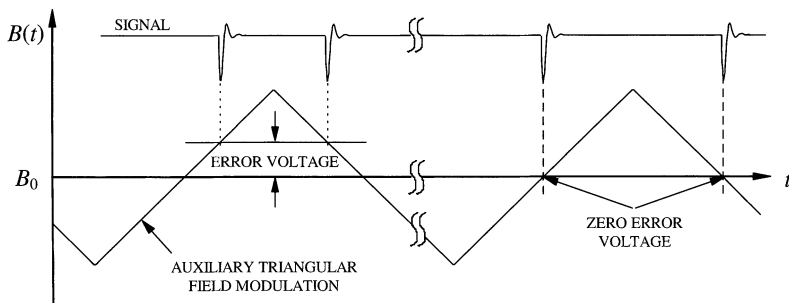
FIGURE 3   NMR signals in standard operation mode; before (left) and after (right) fine tuning.

be borne in mind that the clearly visible NMR response is the result of sophisticated electronic filtering and signal processing. The relative amplitude change of the resonant circuit, containing the active material, amounts less than 10^{-3} due to the response of the proton spins. As a consequence of this very small signal variation, the probe is usually AC coupled (to eliminate DC drift problems) to the amplifier chain with a lower cut-off frequency of the order of 10 Hz.

2.3   Electron Spin Resonance (ESR)

A general description of the working principle of the ESR[9] is not given here. Instead the special case of the Ferrimagnetic Resonance (FMR) is discussed below. However, for practical purposes it is worth mentioning that ESR is well suited to filling the gap in the measurement range between very low fields and say 400 G, where small-size NMR probes take over. It should be remembered that 400 G is not really a basic inferior limit for NMR probes but rather the limit of present technology for small probe dimensions (diameter < 5 mm) and reasonable signal-to-noise ratios for measurement periods of less than 1 s. Within the constraints mentioned above, the ESR is a complementary solution to NMR below 400 G and directly compatible with commercially available NMR teslameters.

2.4   Ferrimagnetic Resonance (FMR)

As already mentioned, NMR probes require a homogeneous B-field for valid operation. Known gradients may be compensated to some extent

by gradient correction coils but this method has its limitations. If there is a need to take measurements in inhomogeneous fields by means of a spin resonance device, then one may consider the use of FMR probes.[9] Due to their small probe sizes (diam. down to 0.3 mm) and comparatively low Q-values (~ 1000), considerable gradients can be tolerated. A useful FMR response has even been obtained in a typical accelerator quadrupole magnet.

FMR is an electron spin resonance similar to ESR. It occurs in certain ferrites, which are electrically isolating and thus suited to high-frequency operation. FMR should not be confused with ferromagnetic phenomena, which occur in metallic iron alloys. Electron spin resonance (and thus also FMR) typically has a gyromagnetic ratio of 2.8026 GHz/kG in contrast to the NMR value of 4.2576 MHz/kG.[10] FMR has found widespread applications in microwave equipment such as tuncable oscillators (synthesisers) and electronically tuncable (tracking) filters. Typically Yttrium Iron Garnet (YIG) is used as the active material. In a simplified theory for FMR, which is also valid for ESR, the modulus of the spin vector s of a free electron is given as

$$|s| = \sqrt{s(s+1)}\hbar, \tag{1}$$

where $s = \frac{1}{2}$ is the spin quantum number. The magnetic moment of the electron is then found to be

$$\vec{\mu}_s = -g_s \cdot \frac{e}{2m_0} \cdot s, \tag{2}$$

where g_s is the Landé factor[‡] which amounts 2.0023 for a free electron.

For a free electron in a static magnetic field B_0 two energy levels exist and the spin component s_z in the direction of the field has two possible orientations, either parallel or antiparallel, given by

$$s_z = \pm\frac{1}{2}\hbar. \tag{3}$$

[‡] The Landé factor for a bound electron may be different to the number quoted above by a few 10^{-3} due to crystal lattice interactions and must be determined experimentally for each material.

Thus, the component of the magnetic moment μ_z in the field direction can be obtained as

$$\mu_z = \mp g_s \cdot \frac{e}{2m_0} \cdot s_z = \mp g_s \cdot \frac{e}{2m_0} \cdot \frac{1}{2}\hbar = \mp g_s \cdot \mu_B \cdot \frac{1}{2}, \qquad (4)$$

with the Bohr magneton $\mu_B = 9.2732 \cdot 10^{-24}\,A\,m^{-2}$.

The energy difference ΔE between these two possible orientations of the magnetic moment of the electron is given by

$$\Delta E = g_s \mu_B B_0 = h\nu. \qquad (5)$$

The frequency ν, corresponding to this transition is obtained numerically as

$$\nu(Hz) = 2.8026 \cdot 10^{10} \cdot B_0/T. \qquad (6)$$

The above equation can also be rewritten using the Larmor precession frequency ω_L and the gyromagnetic ratio γ as

$$\omega_L = 2\pi\nu = \gamma \cdot B_0 = \frac{\mu_z}{s_z} B_0. \qquad (7)$$

In general, the Lamor frequency for a ferrite sample of ellipsoidal shape is given by

$$\omega_L = \gamma\mu_0\mu_r[H_0 + H_{A(T)} + (N_T - N_z)M_S], \qquad (8)$$

where H_0 is the unperturbed field, $H_{A(T)}$ the crystal anisotropy field, N_T the transverse demagnetisation factor, N_z the axial demagnetisation factor, M_S the saturation magnetisation, μ_0 $(= 4\pi10^{-7}\,V\,s\,A^{-1}\,m^{-1})$ the permeability of vacuum, and μ_r the relative permeability.

For a polycrystalline sphere, the effective crystal anisotropy field $H_{A(T)}$ vanishes and, with $N_T = N_z = \frac{1}{3}$,

$$\omega_L = \gamma\mu_0\mu_r H_0. \qquad (9)$$

There are also higher-order magnetostatic modes[11] at frequencies ω_n which may lead to a spurious response,

$$\omega_L - \gamma\mu_0\mu_r N_T M_S < \omega_n < \omega_L + \gamma\mu_0\mu_r(0.5 - N_T)M_S. \qquad (10)$$

It can be shown that a linear polarised electromagnetic wave can be decomposed into two counter-rotating circular polarised waves. In the same way, an effective magnetic permeability μ for right- and left-hand polarised waves respectively can be defined,

$$\mu_+ = \mu'_+ - j\mu''_+, \qquad \mu_- = \mu'_- - j\mu''_-. \tag{11}$$

This leads to the propagation constants k_+ and k_- for right- and left-hand circular polarised waves respectively. The wave linked to μ_+ shows the desired resonance response with the resonance frequency being strictly proportional to the external bias field B_0 if $H_{A(T)} = 0$ and if a spherical ferrite sample is considered. It should be noted that the ferrite must be magnetised beyond saturation, otherwise the resonance will be "smeared out" i.e. show a very low Q-value due to spin lattice interactions. Typical values for the saturation magnetisation of YIG materials are between 300 and 1000 G. These values define the lower limit of the measurement range, the upper limit is about 3 T. This corresponds to a resonance frequency of 80 GHz which is a practical limit imposed by present microwave technology. The mechanical layout of such a YIG filter is depicted in Figure 4.

RF energy transfer takes place between two orthogonal, semicircular loops of TEM transmission lines. This prevents unwanted coupling between the loops in case of the absence of the YIG resonance.
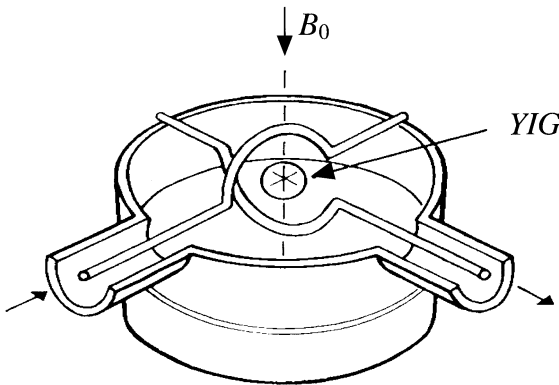

FIGURE 4   Mechanical layout of a YIG filter.

The construction also permits the DC bias field B_0 to be orthogonal to the RF magnetic fields of both coupling loops.

Obviously one would like to obtain the highest possible Q-value for such an FMR filter to be used as a magnetic field sensor. Unfortunately, at this point, conflicting requirements are encountered. The highest performance mono-crystalline ferrites have FMR Q-values exceeding 10 000. However, the alignment of single crystal spheres in a resonator is very delicate and in addition single crystal spheres usually exhibit a strong temperature coefficient of the FMR frequency. This is due to the temperature dependent crystal anisotropy field of such a material. In contrast, polycrystalline spheres do not require any specific alignment as there is no defined crystallographic axis and they have a vanishing temperature coefficient as the internal fields of the grains compensate each other. These effects are shown in Figure 5.[12]

However, the price to be paid is lower Q-values around 1000. Unfortunately, when using common polycrystalline YIG material not even these Q-values are obtained, one has to take calcium substituted
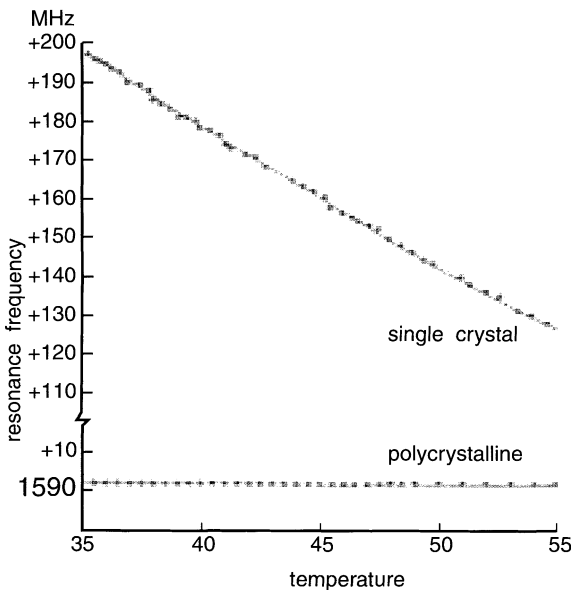

FIGURE 5   Resonance frequency as function of temperature for poly- and single-crystal FMR probes.
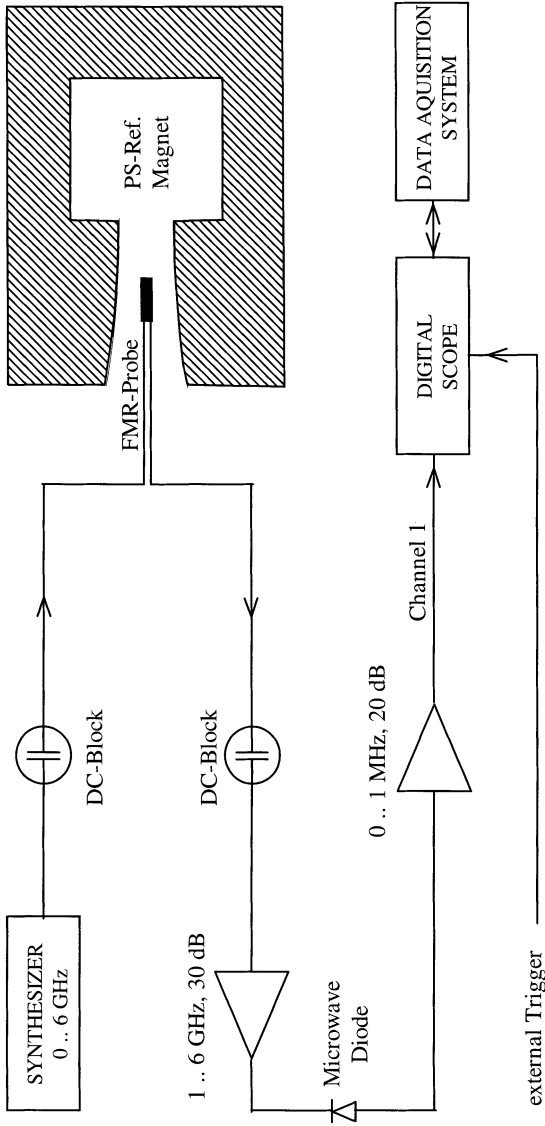
FIGURE 6   Simplified block diagram of the FMR probe in the CERN-PS reference magnet.

YIG and to the authors best knowledge such high-Q polycrystalline spheres have not been produced for about 20 years. At that time they were made by Philips research labs and Raytheon.

In Figure 6 the circuit diagram of the experimental set-up used in the CERN-PS reference magnet is shown. An FMR transmission resonator using a calcium substituted YIG, $Y_{2.4}Ca_{0.6}[Fe_{1.3}In_{0.7}](Fe_{2.7}V_{0.3})O_{12}$ is installed in one of the modules of the PS reference magnet. A frequency synthesiser is set to a programmable, but very stable frequency between 0 and 6 GHz. When the B-field, seen by the YIG sphere corresponds to the Larmor frequency set on the synthesiser, signal transmission within the magnetic window defined by the line-width or Q factor of the FMR material is obtained. The transmitted signal is sent via an amplifier (cable losses) to a detector diode and subsequently to a data acquisition system.

3 SPECIAL MEASUREMENT TECHNIQUES

Due to the particular constraints imposed by the accelerator environment, special NMR and FMR measurement techniques have been elaborated. These constraints make it necessary to measure on flat tops with durations of the order of 100 ms as well as in a dynamic mode during a ramp. NMR measurements on a ramp require only a minor modification of commercially available teslameters.

As described above, the essential part of the measurement process is the auxiliary, triangular magnetic field modulation (see Figure 3). For the measurement process, the origin of this time-dependent field variation is irrelevant. When operating in the "marker-mode" on a ramp, the auxiliary field modulation is turned off and substituted by the dB/dt of the ramp. The internal VCO of the teslameter is disconnected from the probe and replaced by an external frequency synthesiser. This synthesiser is set to a frequency corresponding to the desired field level of the marker, which is defined by the gyromagnetic ratio of protons (4.257608 MHz/kG). Thus the working principle is essentially equivalent to the standard operation mode except that only a single NMR response is obtained when the ramping field traverses the marker level in either direction. The amplified and filtered NMR response is available from an auxiliary output of the teslameter and can subsequently be used

for observation and/or further applications (e.g. to provide a trigger pulse). The typical response taken in the knee region of a rising ramp is similar to the NMR signal shown in Figure 3.

However, the width as well as the height of the NMR response depend on the slew rate of the magnetic field. As mentioned earlier, there is no response to a static field due the AC-coupled electronics. The line-width of the NMR probe for slew rates of less than 1 kG/s is typically of the order of less than 10^{-4} of the field level. For increasing ramp rates, the line-width increases and at the same time the signal amplitude decreases. This is partially due to the band-pass characteristics of the amplifier chain, but also due to intrinsic properties of the NMR probe. However, useable signals have been obtained for slew rates of up to 40 kG/s.

For NMR measurements on flat tops of short duration (less than 0.5 s), the teslameter fine tuning loop (see Figure 3) has insufficient time to lock and a manually operated reading technique, similar to the configuration used in the marker mode, has been adopted. For the time being, it is assumed that the flat top is really flat (which is often not the case). However, it should be noted that the unavoidable 300 or 600 Hz residual field ripple acts in a way similar to the auxiliary field modulation of the teslameter. The NMR marker level is set slightly above the expected flat-top value and then manually changed (tuning of the external synthesiser) until the first peaks of the mains ripple (on the flat top) become visible. The corresponding frequency is noted and defines the upper boundary for the magnetic field on the flat top. To define the lower boundary, the same procedure is applied from a starting value slightly below the expected flat-top level. The magnetic field on the flat top is then defined by the mean value between the upper and lower boundaries.

In contrast to the NMR probes discussed above, FMR probes return a much larger signal strength variation at resonance. This is due to the much higher magnetic moment of the electron as compared to the proton (cf. Eq. (2)). An FMR probe can be seen as a narrow band transmission resonator filter in the microwave region. The relative amplitude change of this resonant circuit amounts more than a factor of 10 (in voltage) compared to 10^{-3} for the NMR. This excellent signal ratio allows DC-coupled electronics after the microwave detection circuit (simple microwave diode detector) and gives a static response over flat tops of any duration without auxiliary field modulation.

4   APPLICATIONS

Absolute *in situ* Calibration of the Integral Bending Field in Circular Machines

It is often desirable to carry out an absolute field calibration in circular machines. Traditionally, this is done using the beam as a field probe and applying basic relationships between revolution frequency, momentum, orbit length and integral bending field. However, this method is tedious and time consuming. Nevertheless, it has to be carried out only once in order to establish experimentally a relationship between the integral field, seen by the beam, and a point measurement in a reference magnet. Therefore, reliable magnetic markers (for the reference magnet), with excellent long-term stability and reproducibility can considerably reduce the calibration effort. As an example, the CERN PS-Booster bending field has been examined, using the concept mentioned above by applying an NMR probe as point-like field marker.[13] The measurements were based on two geometrical parameters:

- Machine circumference (on central orbit): $l_{c.o.} = 50\pi$ m.
- Effective magnetic length of main dipole: $l_{eff} = 1.6177$ m.

In the following, it is assumed that the geometric length of the Booster circumference is well defined and not perturbed by, e.g., thermal dilation. In the PS-Booster, there are 32 main dipole magnets. This gives a total bending length of 51.7664 m for one full turn in the machine and a bending radius ρ of 8.2389 m. For a proton beam with a kinetic energy E, following the central orbit, the revolution frequency f_{rev} is then found to be

$$f_{rev} = \frac{c}{l_{c.o.}} \cdot \sqrt{1 - \left(\frac{m_0 c^2}{E + m_0 c^2}\right)^2}, \qquad (12)$$

where c is the velocity of light and m_0 is the rest mass of the proton. The bending field required to keep the beam on the central orbit is given by

$$B = \frac{E + m_0 c^2}{c\rho} \cdot \sqrt{1 - \left(\frac{m_0 c^2}{E + m_0 c^2}\right)^2}. \qquad (13)$$

TABLE I   Relation between NMR data and beam mesured field levels

Energy [GeV]	RF-h = 5 [MHz]	Field (beam) [G]	Field (NMR) [G]	$(B_{NMR} - B_{beam})/B_{beam}$
0.04977	2.99058	1253.6	1253.4	−1.9E−4
0.05434	3.11416	1311.5	1311.2	−2.2E−4
0.40000	6.80447	3863.5	3862.7	−2.0E−4
0.60000	7.56199	4935.3	4934.0	−2.5E−4
0.80000	8.03314	5924.4	5923.0	−2.3E−4
1.00000	8.35010	6866.7	6865.4	−1.8E−4
1.20000	8.57492	7779.2	7779.0	−0.2E−4
1.30000	8.66377	8227.4	8228.3	1.2E−4

As the radio-frequency is measured with a high precision (ppm level), the above formulae can be used to determine the beam energy and the (integrated) bending field. Starting from the central orbit length, RF frequencies corresponding to certain beam energies (quoted in Table I) were calculated and magnetic cycles with flat tops at these energies were programmed (in 1997 the Booster RF system made use of the fifth harmonic of the revolution frequency). The beam was accelerated up to the various flat-top energies where the RF frequency was fixed (no radial loop, fixed phase). The mean radial position of the beam was then measured with the 16 closed-orbit pick-ups. The field level in the main bending magnets was then adjusted by changing the current of the main power supply, in order to get zero mean radial offset for the beam. The actual beam energy and the bending field were then calculated using (12) and (13).

A second, independent measurement of the actual bending field was performed by means of the NMR probes in the reference magnet. Due to the short duration of the flat tops, a special technique, as described above, had to be used. A third set of data for the B-field was obtained using the B-train[§] measurement (produced via a long pick-up coil in the reference magnet) of the Booster.

Results

The various beam energies for which measurements were carried out and the corresponding RF frequencies are listed in Table I. The field levels measured with the beam and with the NMR Teslameter

---

[§] B-train is an achronym for a real-time distribution system of the time dependent B-field, using one pulse for a defined increment (e.g. 1 pulse per Gauss).

respectively as well as the relative deviation between both measurements with respect to the beam related data are quoted.

The absolute and relative differences of the B-field data obtained with the NMR teslameter and the beam are shown in Figure 7. The most likely explanation of the behaviour of the residual field difference between these measurements (see Figure 7) is the non-linear dependence of the effective magnetic length on the field level. It should be kept in mind that the NMR probe is a point-like measurement in the homogeneous region of the reference magnet, whereas the beam really "sees" the integrated field around the circumference of the machine.

Comparison between NMR and B-train

Table II shows a comparison between NMR probe data, the measured B-train and the B-field (evaluated with the beam) as a function of energy.

As is evident from Table II, the measured B-train produced via a long pick-up coil in the reference magnet, followed by a voltage to
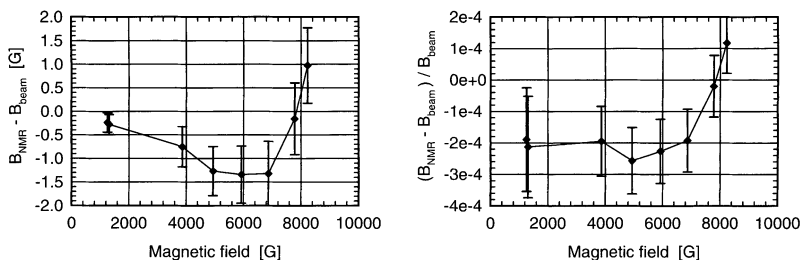

FIGURE 7   Absolute and relative differences of B-field data obtained with NMR and beam.

TABLE II   Comparison of B-field data obtained via NMR probe, B-train and beam measurement

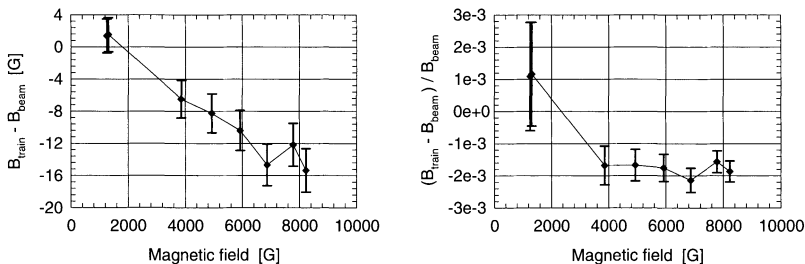| Energy [GeV]	Field (beam) [G]	Field (NMR) [G]	Field (B-train) [G]
0.04977	1253.6	1253.4	1255
0.05434	1311.5	1311.2	1313
0.40000	3863.5	3862.7	3857
0.60000	4935.3	4934.0	4927
0.80000	5924.4	5923.0	5914
1.00000	6866.7	6865.4	6852
1.20000	7779.2	7779.0	7767
1.30000	8227.4	8228.3	8212

FIGURE 8   Absolute and relative differences of *B*-field data obtained with *B*-train and beam.

frequency-converter-based integrator, shows a discrepancy (increasing with energy) with respect to the *B*-field data obtained by beam and NMR measurements. This is most likely to be attributed to a gain and/ or off-set error in the analog electronics of the *B*-train generator. The differences between the *B*-train and the data obtained by the beam measurement are shown in Figure 8.

Synthetic *B*-train with Magnetic Markers

In contrast to the method described above, a similar looking *B*-train can be generated (without using a pick-up coil) by means of a numerical magnet model. This model is sometimes called "synthetic *B*-train generator". This synthesised train generator delivers output pulses at fixed moments in time, corresponding to the power supply control values.

The remanent field acts like an unknown off-set to the system and should be determined via a magnetic measurement on or near flat bottom. Imperfections of the magnetic model (non-linearity) as well as long-term drifts of the output current make the use of a second marker near the flat top desirable.

5   CONCLUSIONS

A review of different magnetic marker systems that are currently in use in the accelerator environment has been given. The advantages and disadvantages of the different techniques were discussed. The use of magnetic markers has led to significant improvements in both the

long-term stability and the precision of magnetic field measurements in ramped machines. The present paper mainly focuses on marker techniques relying on nuclear or electron spin resonance probes (NMR, ESR, FMR). The main advantages of probes of these kinds are their high accuracy and long-term stability. They are also insensitive to alignment errors (tilts) relative to the magnetic field to be measured. However, a common drawback (except for FMR) is the need for a high degree of field homogeneity.

Acknowledgements

References

[1] P. Di Cesare, C. Reymond, H. Rottstock and P. Sommer, SPS magnetic field cycle measurement system, SPS/PCO/Note 89-9, 1989.
[2] Ch. Schott and R.S. Popovic, Hall transducer for high precision magnetic field measurements from DC to 100 kHz, *Proceedings of the 10th International Magnet Measurement Workshop*, Vol. 2, Fermilab, 1997.
[3] J.M. Kelly, Magnetic field measurements with peaking strips, *Rev. Sci. Instr.*, **22**, 256–258, 1951.
[4] G.K. Green, R.R. Kassner, W.H. Moore and L.W. Smith, Magnetic measurements, *Rev. Sci. Instr.*, **24**, 743–754, 1953.
[5] R. Gabillard, Notes sur la fabrication des 'peaking strips', CERN-PS/RGb 10, Avril 1957.
[6] F. Hartmann, Resonance magnetometers, *IEEE Trans. on Magn.*, MAG-8, 66–75, 1972.
[7] *NIST Journal*, Vol. 95, Nb. 5, p. 521, Sept.–Oct. 1990.
[8] F. Bordry, H.K. Kuhn, J.D. Pahud and H. Rottstock, Mesures de l' induction magnetique au niveau des cycles leptons du SPS par sonde NMR, SPS/AOP/Note 88-5, 1988.
[9] H. Weiss, Messung von Magnetfeldern, in Handbuch der Physik, Bd. XXIII, Ed. A.E. Pannenborg.(Springer Verlag), 1967.
[10] N. Kernevez, D. Duret, M. Moussavi and J.M. Leger, Weak field NMR and ESR spectrometers and magnetometers, *IEEE Trans. on Magn.*, **28**(5), 3054–3059, 1992.
[11] Meinke and Grunlach, Taschenbuch der Hochfrequenztechnik, 4th edn., Chap. 9.8, Eds. K. Lange, K.H. Löcherer (Springer Verlag), 1985.
[12] F.K. Beckmann, H. Dötsch, P. Röschmann and W. Schilz, Remote temperature sensing in organic tissue by ferrimagnetic resonance frequency measurements, 11th European Microwave Conference, Amsterdam (Microwave Exhibitions and Publishers Ltd.), 1981.
[13] M. Benedikt, F. Caspers, T. Salvermoser, Absolute calibration of the CERN PS-booster bending field with beam and NMR, PS/OP/Note 98-23, 1998.